Distributed Massive MIMO FMCW Radar Simulator based on Ray Tracing

Moein Ahmadi, Mohammad Alaee-Kerahroodi, Bhavani Shankar M. R., and Björn Ottersten
Interdisciplinary Centre for Security, Reliability and Trust (SnT), University of Luxembourg
moein.ahmadi@uni.lu, mohammad.@uni.lu, bhavani.shankar@uni.lu, bjorn.ottersten@uni.lu

ABSTRACT

This work introduces a system-level model for radar signal generation, developed to support the latest applications of radar technology like automotive radar industry, high-resolution RF security screening and vital sign monitoring. This study models the dynamic environmental geometry sourced from conventional 3D software such as Blender. Subsequently, it introduces a ray tracing approach incorporating multipath reflections and line of sight based ray allocation to accurately compute the delay and amplitude of received signals based on the radar equation. The proposed model supports a range of conventional multichannel FMCW radar techniques, including phased array, slow time TDM, BPM, DDM MIMO radar for the generation of received signals. The simulation results from the CUDA GPU-accelerated implementation demonstrate the capabilities of the proposed radar signal simulator.

Index Terms— Distributed MIMO radar, indoor sensing, mmWave FMCW radar, radar heart sound, security screening.

I. INTRODUCTION

Radar sensors play a key role in advancing autonomous driving technology, providing reliable object detection even in challenging conditions [1]. Another emerging application of radar technology involves the proposal for massive MIMO radar systems in passenger screening. These systems use millimeter-wave frequencies that, unlike X-rays and other forms of ionizing radiation, do not penetrate the skin or disrupt cellular or DNA structures [2]. Authors in [3] consider a co-located massive MIMO radar and explore the potential benefits of having a large number of virtual spatial antenna channels. In most of these applications, the designs require arrays that comprise a large number of virtual array elements.

Simulating radar data offers numerous advantages, including the ability to test and assess diverse antenna configurations, optimized for specific arrays, in more realistic scenarios prior to fabricating a physical prototype. Additionally, testing innovative algorithms in user-defined scenarios is often more feasible with simulated data than with actual measurements. Radar simulations are also valuable for generating data require for training machine learning algorithms [4].

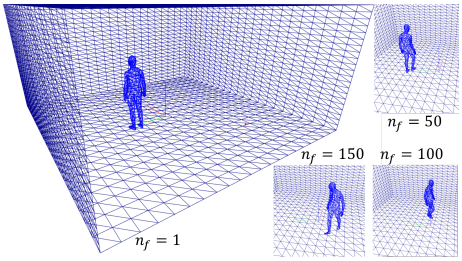

Fig. 1: Dynamic sensing environment with 5455 triangles and multiple frames

Besides hardware radar signal emulators, there are several approaches to simulating radar sensor data, including methods based on physical models, scattering centers models, and data-driven models [5]. Similar to [6], this paper utilizes a physical model based on the Shooting and Bouncing Rays (SBR) technique. This paper introduces a radar ray tracing approach initialized by a ray allocation algorithm that generates a single ray for each target located within the line of sight of the transmitting element. Furthermore, it calculates the amplitude of the received paths using a modified radar equation, accounting for both monostatic and bistatic Radar Cross Section (RCS) values of the targets. Contrary to [6], the proposed simulator in this work has the capability to simulate multi-suite, multi-radar configurations. This allows for the modeling of interference from other radar sensors present in the scene. The comprehensive end-to-end system model of the proposed simulator enables it to generate signal data for the most recent radar applications. This includes applications like RF microphones for vital sign monitoring, which utilize the unwrapped phase derived from chest's skin vibrations caused by heart sounds [7].

The paper outlines geometric modeling and radar ray tracing in section II. The radar signal generation is described in section III. Section IV contains the simulation results. Finally, conclusions are drawn in section V.

II. GEOMETRIC MODEL AND RAY TRACING

We consider a dynamic scenario which contains N_f time frames of an environment that consists N_{obj} objects and each object contains $N_{tri,n_{obj}}$ triangles, $T_{n_f,n_{obj},n_{tri}}$, where $n_{obj} = 1, \ldots, N_{obj}$. Each triangle is defined by an origin

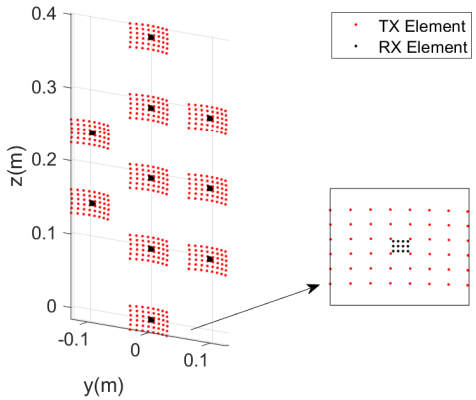

Fig. 2: Radar sensor with 480 TX, 120 RX Elements, 57600 virtual array elements

vector $\mathbf{o}_{n_f,n_{obj},n_{tri}}$ and two side vectors $\mathbf{u}_{n_f,n_{obj},n_{tri}}$ and $\mathbf{v}_{n_f,n_{obj},n_{tri}}$ where $n_f = 1,\ldots,N_f$, as shown in Fig. 1.

In a sensing scenario, there are N_V vehicles(or suites) and each vehicle consists N_{radar,n_V} coherent multichannel radar sensors where $n_V = 1,\ldots,N_V$. Each coherent multichannel radar sensor has $M^t_{n_v,n_r}$ transmit antenna elements and $M^r_{n_v,n_r}$ receive antenna elements. Fig. 2 shows a multichannel radar sensor with $M^t_{n_v,n_r} = 480$ and $M^r_{n_v,n_r} = 120$. In each time frame, the antenna position and beampattern direction are represented as $\mathbf{p}^t_{n_f,n_v,n_r,m_t}$ and $\mathbf{d}^t_{n_f,n_v,n_r,m_t}$ for the transmit, and $\mathbf{p}^r_{n_f,n_v,n_r,m_r}$ and $\mathbf{d}^r_{n_f,n_v,n_r,m_r}$ for the receive antenna elements, within the World Coordinate System (WCS).

II-A. Simulator coordinate systems

To convert from the Sensor Coordinate System (SCS) and Vehicle Coordinate System (VCS) to the WCS, transformation matrices can be employed. If $\mathbf{R}_{sv}$ and $\mathbf{t}_{sv}$ are the rotation matrix and translation vector from SCS to VCS and $\mathbf{R}_{vw}$ and $\mathbf{t}_{vw}$ are the rotation matrix and translation vector from VCS to WCS, to convert directly from the SCS to the WCS, the two transformations can be combined as

$$\mathbf{p}^{[1]}_{wcs} = \mathbf{G}_{vw}\mathbf{G}_{sv}\mathbf{p}^{[1]}_{scs} \tag{1}$$

where $\mathbf{x}^{[1]}$ is the vector $\mathbf{x}$ with a 1 appended to it, and

$$\mathbf{G}_{sv} = \begin{bmatrix} \mathbf{R}_{sv} & \mathbf{t}_{sv} \\ 0 & 1 \end{bmatrix}, \mathbf{G}_{vw} = \begin{bmatrix} \mathbf{R}_{vw} & \mathbf{t}_{vw} \\ 0 & 1 \end{bmatrix} \tag{2}$$

II-B. Radar ray tracing

The primary objective of radar ray tracing is to determine the ray paths from the transmit to the receive antenna elements, focusing specifically on calculating their **amplitude**, **distance**, and **distance rate**. This information is essential for the generation of the radar signal.

A ray $\mathbf{r}(t)$ is parameterized by a scalar t and is defined by $\mathbf{r}(t) = \mathbf{o} + t\mathbf{d}$, which $\mathbf{o}$ is the origin of the ray and $\mathbf{d}$ is the direction vector of the ray, typically normalized to have a magnitude of 1. The fundamental operation employed in ray tracing is raycasting, which involves calculating the intersection of a ray with a triangle.

As outlined in Algorithm 1, ray tracing commences by assigning rays to each transmit antenna element.

Algorithm 1 Ray Allocation for Transmit Antenna Element

1: Uniformly distribute rays across azimuth and elevation angles.
2: Identify triangles that are in the line of sight of the transmit antenna element.
3: **for** each triangle in the line of sight **do**
4: Allocate a ray directed towards the center of the triangle.
5: **end for**
6: Compute the number of rays intersecting each triangle.
7: **Output**: Array of rays $\mathbf{r}^0_{n_f,n_v,n_r,m_t,h}$, where $h = 1,\ldots,N^{Ray,0}_{n_f,n_v,n_r,m_t}$, and the count of intersections for each triangle $c_{n_f,n_v,n_r,m_t,n_{obj},n_{tri}}$.

Algorithm 2 outlines the radar ray tracing. Initially, rays are designated to each transmitting antenna element based on the results from Algorithm 1. For every subsequent bounce, the algorithm evaluates intersections for each ray from the preceding bounce. A ray might either intersect with a single triangle or not intersect any. When a ray intersects triangle T_{n_f,n_0,k_0}, the intersection point is identified as $\mathbf{o}^1_{n_f,n_v,n_r,m_t,h'}$. This leads to the generation of a set of new rays for the next bounce. In the most basic scenario, this set includes a ray directed in the triangle's reflection direction. This direction is calculated as

$$\begin{aligned}\mathbf{d}^1_{n_f,n_v,n_r,m_t,h'} &= \mathbf{d}^0_{n_f,n_v,n_r,m_t,h} \\ &- 2(\mathbf{d}^0_{n_f,n_v,n_r,m_t,h}\mathbf{n}_{n_f,n_0,k_0})\mathbf{n}_{n_f,n_0,k_0}\end{aligned} \tag{3}$$

with $\mathbf{n}_{n_f,n_0,k_0} = \frac{\mathbf{u}_{n_f,n_0,k_0}\times\mathbf{v}_{n_f,n_0,k_0}}{|\mathbf{u}_{n_f,n_0,k_0}\times\mathbf{v}_{n_f,n_0,k_0}|}$ denoting the normal vector of the intersected triangle. For every intersection point, if there is a line of sight to a receive antenna element, Algorithm 2 generates a new corresponding path. Following the completion of the while loop in the algorithm, which includes the N_{Bounce} iterations, for the m^{th}_r receive antenna element of the n^{th}_r radar on the n^{th}_v vehicle, there exist $n_p = 1,\ldots,N_{P,n_f,n_v,n_r,m_r}$ paths. The power, distance, and distance rate of these paths are required for the generation of the radar signal and calculated in the following subsections. For the n^{th}_p path, the variables $n'_v = n^v_{n_f,n_v,n_r,m_r,n_p}$, $n'_r = n^r_{n_f,n_v,n_r,m_r,n_p}$, and $m'_t = m^t_{n_f,n_v,n_r,m_r,n_p}$ respectively represent the vehicle, radar, and transmit element index corresponding to the source ray of the path. Additionally, $n^o_{n_s}$ and $n^t_{n_s}$ (where $n_s = 1,\ldots,N_{s,n_f,n_v,n_r,m_r,n_p} - 1$) denote the object and triangle indices respectively for the current path sequence. If $n'_v = n_v$ and $n'_r = n_r$, then the transmit signal originates from the same device as the receive antenna element currently under analysis, otherwise

the transmit signal should be considered as interference for the receive antenna element.

Algorithm 2 Radar Ray Tracing Algorithm

Allocate transmit rays, $\mathbf{r}^0_{n_f,n_v,n_r,m_t,h}$, where $h = 1,\ldots,N^{Ray,0}_{n_f,n_v,n_r,m_t}$ for each transmit antenna element.
Initialize bounce iteration, $b \leftarrow 1$.
while $b \leq N_{Bounce}$ **do**
  for all $\mathbf{r}^{b-1}_{n_f,n_v,n_r,m_t,:}$ **do**
    Identify intersected rays, $\mathbf{r}^b_{n_f,n_v,n_r,m_t,h}$; $h = 1,\ldots,N^{Ray,b}_{n_f,n_v,n_r,m_t}$, and their source ray, source triangle, and hit triangle indices.
    Calculate distance and distance rate.
    for all Receive antenna elements **do**
      if $\mathbf{o}^b_{n_f,n_v,n_r,m_t,h}$ has line of sight with the receive antenna element **then**
        Calculate distance and distance rate to the receive antenna element and create a new path for this receive antenna element.
      end if
    end for
  end for
  Increment bounce iteration, $b \leftarrow b+1$.
end while

II-C. Path distance

The distance related to a path can be easily calculated $d_{n_f,n_v,n_r,m_r,n_p} = \sum_{n_s=1}^{n_s=N_{s,n_f,n_v,n_r,m_r,n_p}} d_{n_f,n_v,n_r,m_r,n_p,n_s}$, where $d_{n_f,n_v,n_r,m_r,n_p,1} = |\mathbf{o}_{n_f,n^o_1,n^t_1} - \mathbf{p}^t_{n_f,n'_v,n'_r,m'_t}|$, $d_{n_f,n_v,n_r,m_r,n_p,end} = |\mathbf{p}^r_{n_f,n_v,n_r,m_r} - \mathbf{o}_{n_f,n^o_{end},n^t_{end}}|$ and for $n_s = 2,\ldots,N_{s,n_f,n_v,n_r,m_r,n_p}-1$, it is $d_{n_f,n_v,n_r,m_r,n_p,n_s} = |\mathbf{o}_{n_f,n^o_{n_s},n^t_{n_s}} - \mathbf{o}_{n_f,n^o_{n_s-1},n^t_{n_s-1}}|$.

II-D. Path power

Through a path, when a triangle encounters an electromagnetic wave, the energy from the wave scatters in multiple directions based on the triangle's RCS pattern. Notably, a portion of this incident power is backscattered, meaning it is re-emitted in the direction of the incident ray. It is assumed that the most potent reflection occurs in the direction corresponding to the triangle's reflection in (3) which considered as triangle's bistatic radar cross section, $\sigma^{bs}_{n_f,n_{obj},n_{tri}}$. For directions deviating from the triangle's reflection direction, the triangle's RCS pattern $\sigma^{(\theta,\phi)}_{n_f,n_{obj},n_{tri}}$ or for simplicity monostatic radar cross section, $\sigma_{n_f,n_{obj},n_{tri}}$, can be applied. A related measure, the Normalized Radar Cross-Section (NRCS), proves to be insightful. For backscatter and bistatic instances, this is represented as σ^0 and $\sigma^{0,bs}$, respectively. With the aid of the NRCS, the relation $\sigma^{bs}_{n_f,n_{obj},n_{tri}} = \sigma^{0,bs}_{n_{obj},n_{tri}} A_{n_f,n_{obj},n_{tri}}$ is established, where $A_{n_f,n_{obj},n_{tri}} = \frac{1}{2}|\mathbf{u}_{n_f,n_{obj},n_{tri}} \times \mathbf{v}_{n_f,n_{obj},n_{tri}}|$ represents the triangle's area. the associated received power for the path is calculated by

$$P^r_{n_f,n_v,n_r,m_r,n_p} = \frac{P^t_{n'_v,n'_r,m'_t} G^{t,(\theta_t,\phi_t)}_{n'_v,n'_r,m'_t}}{4\pi d^2_{n_f,n_v,n_r,m_r,n_p,(n_s=1)}} \times \left(\Pi_{n_s=2}^{N_{s,n_f,n_v,n_r,m_r,n_p}-1} \frac{\sigma^{bs}_{n_f,n^o_{n_s-1},n^t_{n_s-1}}}{4\pi d^2_{n_f,n_v,n_r,m_r,n_p,n_s}}\right) \times \frac{\sigma_{n_f,n^o_{N_{s,n_f,n_v,n_r,m_r,n_p}-1},n^t_{N_{s,n_f,n_v,n_r,m_r,n_p}-1}}}{4\pi d^2_{n_f,n_v,n_r,m_r,n_p,N_{s,n_f,n_v,n_r,m_r,n_p}}} \frac{G^{r,(\theta_r,\phi_r)}_{n_v,n_r,m_r}\lambda^2}{4\pi} \quad (4)$$

It is important to note that the RCS for the triangle which intersected by transmit antenna element ray is divided by $c_{n_f,n_v,n_r,m_t,n^o_{n_s=1},n^t_{n_s=1}}$. In (4), $G^{t,(\theta,\phi)}_{n'_v,n'_r,m'_t}$ and $G^{r,(\theta,\phi)}_{n_v,n_r,m_r}$ are the transmit and receive antenna element gain in the direction of azimuth, θ, and elevation, ϕ, angles in SCS for the corresponding ray.

II-E. Path distance rate

To generate the radar signal incorporating micro motion and Doppler effects, the path distance rate is computed using the position data obtained from the subsequent frame. The path distance rate can be calculated as $v_{r,n_f,n_v,n_r,m_r,n_p} = \sum_{n_s=1}^{n_s=N_{s,n_f,n_v,n_r,m_r,n_p}} v_{r,n_f,n_v,n_r,m_r,n_p,n_s}$, where

$$v_{r,n_f,n_v,n_r,m_r,n_p,1} = (\mathbf{o}_{n_f+1,n^o_1,n^t_1} - \mathbf{o}_{n_f,n^o_1,n^t_1} - \mathbf{p}^t_{n_f+1,n'_v,n'_r,m'_t} + \mathbf{p}^t_{n_f,n'_v,n'_r,m'_t}) \times \frac{\mathbf{o}_{n_f,n^o_1,n^t_1} - \mathbf{p}^t_{n_f,n'_v,n'_r,m'_t}}{d_{n_f,n_v,n_r,m_r,n_p,1}} f_{fps}$$

$$v_{r,n_f,n_v,n_r,m_r,n_p,\text{end}} = f_{fps}(\mathbf{p}^r_{n_f+1,n_v,n_r,m_r} - \mathbf{p}^r_{n_f,n_v,n_r,m_r} - \mathbf{o}_{n_f+1,n^o_{\text{end}},n^t_{\text{end}}} + \mathbf{o}_{n_f,n^o_{\text{end}},n^t_{\text{end}}}) \times \frac{\mathbf{p}^r_{n_f,n_v,n_r,m_r} - \mathbf{o}_{n_f,n^o_{\text{end}},n^t_{\text{end}}}}{d_{n_f,n_v,n_r,m_r,n_p,N_{s,n_f,n_v,n_r,m_r,n_p}}}$$

and for $n_s = 2,\ldots,N_{s,n_f,n_v,n_r,m_r,n_p}-1$, it is

$$v_{r,n_f,n_v,n_r,m_r,n_p,n_s} = f_{fps}(\mathbf{o}_{n_f+1,n^o_{n_s},n^t_{n_s}} - \mathbf{o}_{n_f,n^o_{n_s},n^t_{n_s}} - \mathbf{o}_{n_f+1,n^o_{n_s},n^t_{n_s-1}} + \mathbf{o}_{n_f,n^o_{n_s},n^t_{n_s-1}}) \times \frac{\mathbf{o}_{n_f,n^o_{n_s},n^t_{n_s}} - \mathbf{o}_{n_f,n^o_{n_s},n^t_{n_s-1}}}{d_{n_f,n_v,n_r,m_r,n_p,n_s}}$$

where f_{fps} is the animation frame rate.

III. RADAR SIGNAL GENERATION

III-A. Radars and frames timing

The animation frame start time is denoted as t^{anim}_{start}. For frame n_f, the simulation begins at $t^{anim}_{n_f} = t^{anim}_{start} + (n_f-1)/f_{fps}$ and lasts for a duration of $1/f_{fps}$ seconds. A radar is operational from $t^0_{n_v,n_r}$. If $t^0_{n_v,n_r}$ is later than $t^{anim}_{n_f}$, the radar's operational time, t_{n_v,n_r}, starts at $t^0_{n_v,n_r}$.

With each pulse n_{pulse}, the time increments by $\mathbf{\Delta}^{i}_{n_v,n_r}$, where $i = (n_{pulse} - 1 \mod N_{\mathbf{\Delta},n_v,n_r}) + 1$. This implies $\tau_{n_v,n_r,n_{pulse}+1} = \tau_{n_v,n_r,n_{pulse}} + \mathbf{\Delta}^{i}_{n_v,n_r}$. Here, $\mathbf{\Delta}_{n_v,n_r}$ represents the Pulse Repetition Interval (PRI) sequence with length $N_{\mathbf{\Delta},n_v,n_r}$ for various PRI modulations such as constant, jittered, staggered, and dwell-and-switch modulations.

Some of the parameters utilized in the subsequent sections of this paper are detailed here as $M^{p}_{n_v,n_r}$ is multichannel precoding pulse number, $\tau_{n_v,n_r,n_{pulse}}$ is absolute start chirp time for each pulse, $\phi^{carrier}_{n_v,n_r}$ is transmit oscillator carrier phase, $h^{filter}_{n_v,n_r}(f)$ is baseband RX filter frequency response, B_{n_v,n_r,m_r} is baseband receiver filter bandwidth, f_{0,n_v,n_r} is central frequency, T_{s,n_v,n_r,m_r} is system noise temperature, β_{n_v,n_r,m_r} is receiver input impedance, $t^{anim}_{n_f}$ is environment animation time, t_{n_f,n_v,n_r} is radar time for each frame, $PRI^{mean}_{n_f,n_v,n_r}$ is average PRI for PRI Modulation, F_{s,n_v,n_r} is ADC sampling frequency, $T^{ADC}_{n_v,n_r}$ is ADC sampling duration, $k^{FM}_{n_v,n_r}$ is FM slope rate, c is light speed and $u(.)$ is unit step function.

III-B. Multichannel precoding matrix

In multichannel FMCW radars, Time Division Multiplexing (TDM), Binary Phase Modulation (BPM), Doppler Division Multiplexing (DDM), and phased array can be implemented. The slow time precoding matrix, denoted as $\mathbf{W}_{n_v,n_r} \in \mathbb{C}^{M^{p}_{n_v,n_r} \times M^{t}_{n_v,n_r}}$, is defined for multiple pulse waveform multiplexing techniques and phased array radars. It is assumed that the magnitude of each matrix element $|w_{n_v,n_r,m_p,m_t}|$ is less than or equal to 1.

In TDM MIMO radar systems, the transmitters emit signals successively in a fixed periodic order. For such a system, the elements of the precoding matrix $w^{TDM}_{n_v,n_r,m_p,m_t}$ are either 0 or 1, where $\sum_{m_t=1}^{M^{t}_{n_v,n_r}} w^{TDM}_{n_v,n_r,m_p,m_t} = 1$ and $\sum_{m_p=1}^{M^{p}_{n_v,n_r}} w^{TDM}_{n_v,n_r,m_p,m_t} \geq 1$. This ensures that each transmitter is active at least once in each cycle, and that there is one active transmitter at any pulse time.

BPM uses Hadamard coding to ensure perfect orthogonality in slow-time. The number of transmit elements and the length of the code are constrained by the inherent properties of the Hadamard matrix, implying that $M^{t}_{n_v,n_r}$, $M^{t}_{n_v,n_r}/12$, or $M^{t}_{n_v,n_r}/20$ must be a power of 2. If $h^{M}_{m,n}$ denotes the element in the m^{th} row and n^{th} column of an $M \times M$ Hadamard matrix, then $w^{BPM}_{n_v,n_r,m_p,m_t} = h^{M^{t}_{n_v,n_r}}_{(m_p \mod M^{t}_{n_v,n_r})+1,m_t}$.

For the DDM technique, the uni-modular precoding weights can be defined as $w^{DDM}_{n_v,n_r,m_p,m_t} = e^{-j2\pi m_p m_t / M^{t}_{n_v,n_r}}$.

The precoding matrix for Phased Array (PA) radar at the specific focusing SCS angles θ_0, ϕ_0 can be expressed by $w^{PA,(\theta_0,\phi_0)}_{n_f,n_v,n_r,m_p,m_t} = e^{j\mathbf{k}^{T}(\theta_0,\phi_0)\mathbf{p}^{t}_{n_f,n_v,n_r,m_t}}$, where $\mathbf{k}$ is the wavenumber vector [8]. It is important to note that in this case, $w^{PA,(\theta_0,\phi_0)}_{n_f,n_v,n_r,m_p,m_t}$ is independent of m_p.

III-C. Raw data generation

Assume the n_r^{th} radar of the n_v^{th} vehicle is a FMCW radar. The transmit signal phase is $2\pi(f_{0,n_v,n_r}(t-\tau_{n_v,n_r,n_{pulse}}) + \frac{1}{2}k^{FM}_{n_v,n_r}(t-\tau_{n_v,n_r,n_{pulse}})^2) - \phi^{carrier}_{n_v,n_r}$. The received antenna signal is multiplied by the transmit signal from the radar, the sum frequency component filtered out and for each path, the signal with the following phase remains

$$\begin{aligned}\phi_{b,n_v,n_r,n'_v,n'_r}(t, d^{n_{pulse},n_{ADC}}_{n_f,n_v,n_r,m_r,n_p}) = 2\pi(&f_{0,n_v,n_r}\\ &(t-\tau_{n_v,n_r,n_{pulse}}) - f_{0,n'_v,n'_r}(t - d^{n_{pulse},n_{ADC}}_{n_f,n_v,n_r,m_r,n_p}/c\\ &- \tau_{n'_v,n'_r,n_{pulse}}) + \frac{1}{2}k^{FM}_{n_v,n_r}(t-\tau_{n_v,n_r,n_{pulse}})^2\\ &- \frac{1}{2}k^{FM}_{n'_v,n'_r}(t - d^{n_{pulse},n_{ADC}}_{n_f,n_v,n_r,m_r,n_p}/c - \tau_{n'_v,n'_r,n_{pulse}})^2)\\ &- \phi^{carrier}_{n_v,n_r} + \phi^{carrier}_{n'_v,n'_r}\end{aligned} \tag{5}$$

where $n_{ADC} = 1, \ldots, N^{ADC}_{n_v,n_r} = \left\lfloor T^{ADC}_{n_v,n_r} F_{s,n_v,n_r} \right\rfloor$, while n_{pulse} is the index for the slow time pulse. Within each frame, the number of pulses is determined by $\left\lceil \frac{t^{anim}_{n_f+1} - t_{n_f,n_v,n_r}}{PRI^{mean}_{n_f,n_v,n_r}} \right\rceil$. Also,

$$\begin{aligned}d^{n_{pulse},n_{ADC}}_{n_f,n_v,n_r,m_r,n_p} = d_{n_f,n_v,n_r,m_r,n_p} + v_{r,n_f,n_v,n_r,m_r,n_p}\\ (\tau_{n_v,n_r,n_{pulse}} - t^{anim}_{n_f} + \frac{n_{ADC}}{F_{s,n_v,n_r}})\end{aligned} \tag{6}$$

(6) calculates the target distance for each slow and fast time sample, facilitating the simulator's ability to produce signals for sophisticated applications. These include the detection of micron-scale chest's skin vibrations resulting from heart sounds. Additionally, the Doppler effect is integrated within this equation.

The ADC samples of the received antenna elements can be expressed as

$$\begin{aligned}x_{n_f,n_v,n_r,m_r,n_{pulse},n_{ADC}} = &\sum_{\substack{n_p=1 \\ n'_v=n^{v}_{n_f,n_v,n_r,m_r,n_p} \\ n'_r=n^{r}_{n_f,n_v,n_r,m_r,n_p} \\ m'_t=m^{t}_{n_f,n_v,n_r,m_r,n_p}}}^{N_{P,n_f,n_v,n_r,m_r}}\\ &w_{n'_v,n'_r,(n_{pulse}-1 \mod M^{t}_{n'_v,n'_r})+1,m'_t} h^{filter}_{n_v,n_r}(\Delta f_{n_v,n_r,n'_v,n'_r})\\ &a_{n_f,n_v,n_r,m_r,n_p} u(n_{ADC} - F_{s,n_v,n_r} d^{n_{pulse},n_{ADC}}_{n_f,n_v,n_r,m_r,n_p}/c)\\ &e^{j\phi_{b,n_v,n_r,n_v,n_r}(n_{ADC}/F_{s,n_v,n_r}, d^{n_{pulse},n_{ADC}}_{n_f,n_v,n_r,m_r,n_p})}\\ &+ \eta_{n_f,n_v,n_r,m_r,n_{pulse},n_{ADC}}\end{aligned} \tag{7}$$

In (7) $a_{n_f,n_v,n_r,m_r,n_p} = \sqrt{\beta_{n_v,n_r,m_r} p_{n_f,n_v,n_r,m_r,n_p}}$.

$\eta_{n_f,n_v,n_r,m_r,n_{pulse},n_{ADC}}$ is the receiver noise with power $P_{Noise,n_v,n_r,m_r} = \beta_{n_v,n_r,m_r} k B_{n_v,n_r,m_r} T_{s,n_v,n_r,m_r}$. Also, $\Delta f_{n_v,n_r,n'_v,n'_r}$ denoting the differential frequency component resulting from the receiver mixer and can be approximated by its start ramp frequency as

$$\begin{aligned}\Delta f_{n_v,n_r,n'_v,n'_r} = &f_{0,n_v,n_r} - f_{0,n'_v,n'_r} -\\ &k^{FM}_{n_v,n_r}(\tau_{n_v,n_r,n_{pulse}} - \tau_{n'_v,n'_r,n'_{pulse}})\end{aligned} \tag{8}$$

The derived values in (7), are initially amplified by the gain of the receiver amplifier, followed by dynamic range improvement function (such as AGC (Automatic Gain Control), A-law, or μ-law curve). Subsequently, these values are quantized in accordance with the ADC quantization levels. For a standard 16-bit ADC, this quantization process can be effectively approximated by a double-to-short data type conversion in programming languages.

III-D. Parallel implementation note

In this research, ray tracing, signal generation, and radar imaging algorithms are implemented using CUDA kernels to maximize High-Performance Computing (HPC) capabilities. From a radar system perspective, the parallel implementation of (7) is particularly noteworthy. Given that (7) is aptly designed for parallel processing and most GPU devices support up to 1024 threads per block, an effective strategy is to allocate 16, 16, and 4 threads across the block axes for fast time ADC samples, slow time samples in a frame, and receive antenna elements, respectively. This configuration can accelerate simulation times by up to 1024 times in optimal scenarios.

IV. SIMULATION RESULTS

This section presents simulations of various scenarios to demonstrate the fundamental capabilities of the proposed signal model and the simulator. Key parameters for these scenarios include a carrier frequency f_0 of 70 GHz, an FM slope k^{FM} of 19.5 MHz/μs, a sampling frequency F_s of 10 MSps, and a pulse repetition interval of 60 μs. To validate the simulation results and showcase the simulator's capabilities, the transmit power is set to a high value, ensuring a high Signal-to-Noise Ratio (SNR).

For the dynamic environment simulation, Fig. 1 presents a scenario crafted in Blender. It features a human walking in a room over 250 frames at a frame rate of 24 frames per second, with each frame comprising 5455 triangles. Fig. 3 displays the range-Doppler map and the multipath effect at frame 150, where the human is specifically 4 meters away from the radar at this frame. In the right figures of Fig. 3, a Moving Target Indicator (MTI) filter is applied to suppress stationary targets. In the subsequent scenario, a distributed sensor suite consisting three massive TDM MIMO radars is deployed for environment sensing, as depicted in Fig. 4a. Each colocated massive MIMO radar, illustrated in Fig. 2, features 480 sparse transmit antenna elements and 120 filled half wavelength distance receive antenna elements in each subarray. Consequently, each radar has 57600 virtual array elements with almost filled half wavelength distances. Fig. 4 presents the imaging results obtained from each of these radars, while Fig. 5 shows the detection outputs of each radar.

Fig. 6a shows the imaging result when using 4 transmit and 4 receive antenna elements, equivalent to a filled rectangle virtual array comprising 16 elements. As demonstrated in

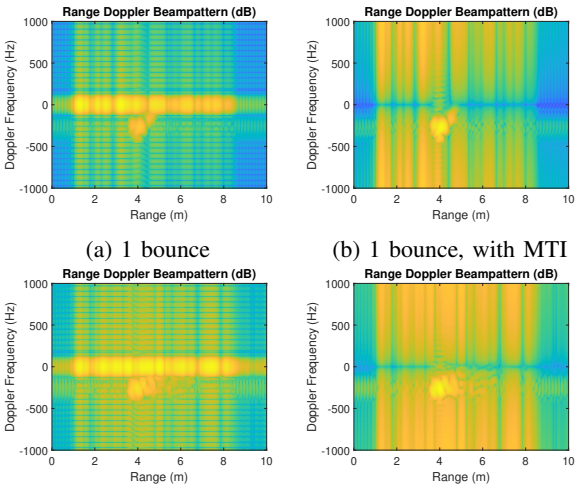

(a) 1 bounce (b) 1 bounce, with MTI

(c) 2 bounces (d) 2 bounces, with MTI

Fig. 3: Range Doppler map (frame 150) and multipath effect

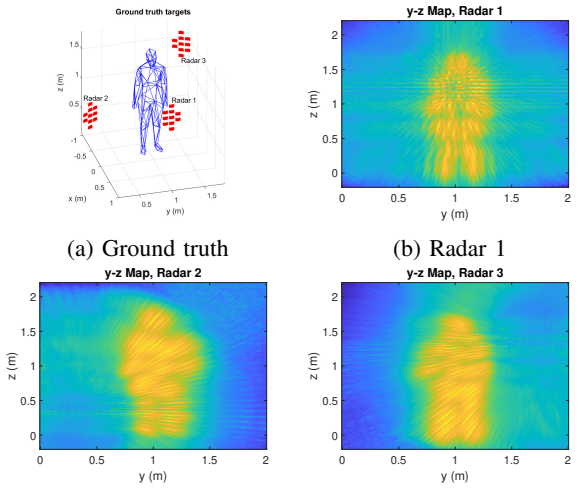

(a) Ground truth (b) Radar 1

(c) Radar 2 (d) Radar 3

Fig. 4: Distributed massive MIMO radar imaging

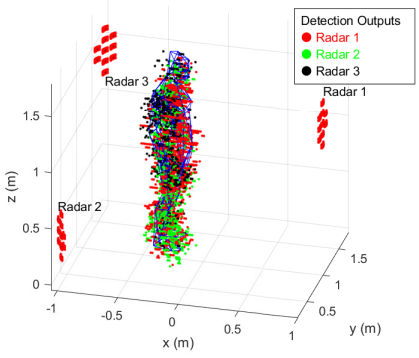

Fig. 5: Detection output in a distributed sensor suite with 3 massive MIMO radars (3×5760 virtual array elements)

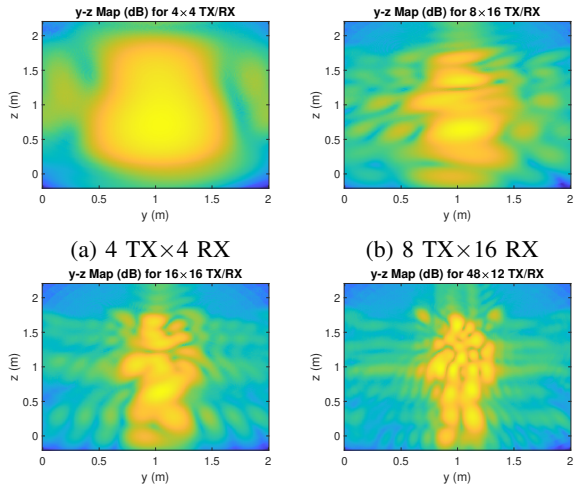

(a) 4 TX×4 RX (b) 8 TX×16 RX

(c) 16 TX×16 RX (d) 48 TX×12 RX

Fig. 6: Cartesian y-z image for some transmit and receive antenna element configurations

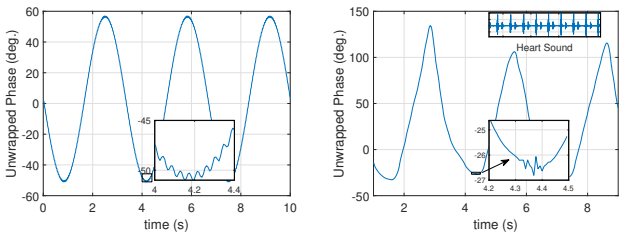

(a) Dual-tone movement model (b) Heart sound + resp. sensor

Fig. 7: Unwrapped phase of the simulated radar signal

Fig. 6, the quality of imaging can be significantly enhanced by increasing the number of transmit and receive elements, leading to a more discernible and detailed human image. The signal model presented in equations (6) and (7) is not only proficient in preserving range, angle, and Doppler information but also excels in maintaining accurate phase information. To illustrate this capability, the final scenario in our study employs this model to validate signal generation in the context of a recent and innovative application in radar cardiography, as detailed in [7]. In this scenario, we model chest movements due to breathing, and micron-scale vibrations caused by heart sounds, using Blender software. Subsequently, the simulator generates the radar signal. The unwrapped phase of the corresponding range gate signal during the slow time is depicted in Fig. 7. In Fig. 7a, a dual-tone movement model is used: one with a low frequency and millimeter-scale movement for breathing, and another with a high frequency and micron-scale movement for heart sound chest's skin vibrations. Both signals are observable in the unwrapped radar signal phase. For a more realistic simulation, chest movement is modeled using data from a Neulog NUL236 respiration monitor belt logger sensor, and chest's skin vibrations are modeled using Emily's heart sound data [9]. As shown in Fig. 7b, the heart sound effect can be seen at small intervals in the unwrapped phase of the radar signal.

V. CONCLUSION

An end-to-end radar system model is presented for multi-suite, distributed, multichannel radar signal generation. It begins with a geometric model of dynamic targets and sensors within a 3D environment, created using Blender software. This is followed by the introduction of a radar ray tracing algorithm, designed to calculate the amplitude and distance for transmit-receive channels. The paper progresses to discuss the timing of animation frames and sensor chips, subsequently introducing the multichannel radar precoding matrix. Subsequently, a signal model for FMCW radar is described, notable for its suitability for parallel implementation. To demonstrate the simulator's capabilities, various recent radar applications are simulated. This research contributes significantly to the advancement of radar technology, offering a versatile and potent tool beneficial to both industry professionals and academic researchers.

VI. ACKNOWLEDGMENT

This work was supported by FNR BRIDGES MASTERS under grant BRIDGES2020/IS/15407066/MASTERS.

VII. REFERENCES

[1] S. Sun, A.P. Petropulu, and H.V. Poor, "MIMO radar for advanced driver-assistance systems and autonomous driving: Advantages and challenges," *IEEE SP Magazine*, vol. 37, no. 4, pp. 98–117, 2020.

[2] Rohde & Schwarz, "R&S QPS QUICK PERSONNEL SECURITY SCANNER," Brochure, 2023, Accessed: November 17, 2023.

[3] S. Fortunati and et all, "Massive mimo radar for target detection," *IEEE Transactions on Signal Processing*, vol. 68, pp. 859–871, 2020.

[4] Arien P. Sligar, "Machine learning-based radar perception for autonomous vehicles using full physics simulation," *IEEE Access*, vol. 8, pp. 51470–51476, 2020.

[5] M. Jasiński, "A generic validation scheme for realtime capable automotive radar sen. models integrated into an auto. driving simulator," in *MMAR*, 2019, pp. 612–617.

[6] C. Schüßler, M. Hoffmann, J. Bräunig, and et al., "A realistic radar ray tracing simulator for large mimo-arrays in automotive environments," *IEEE Journal of Microwaves*, vol. 1, no. 4, pp. 962–974, 2021.

[7] D. Bliss and Y. Rong, "Radar cardiography: A precise cardiac data reconstruction method," U.S. Patent, 2022.

[8] M. Ahmadi, M. Alaee, B. Shankar M. R., and B. Ottersten, "Subspace-based detector for distributed mmWave MIMO radar sensors," in *ICASSP 2023*, 2023, pp. 1–5.

[9] "Emily's heartbeat," Wikipedia: The Free Encyclopedia, 2023, Accessed: November 17, 2023.